Tensile properties of AlCrCoFeCuNi glassy alloys: a molecular dynamics simulation study

Y. Afkham[a], M. Bahramyan[a], R. Taherzadeh Mousavian[a,*], D. Brabazon[b]

[a] *Faculty of Materials Engineering, Sahand University of Technology, Tabriz, Iran*
[b] *Advanced Processing Technology Research Centre, School of Mechanical & Manufacturing Engineering, Dublin City University, Dublin 9, Ireland*

Abstract

High-entropy alloys (HEAs) are among multi-component alloys with attractive microstructures and mechanical properties. In this study, molecular dynamics simulation was used to determine the tensile behaviour of glassy $Al_xCrCoFeCuNi$ HEAs from 300°K to 1300°K. For this purpose, this alloy with variations in chemical concentration of aluminum were heated and then cooled at a high cooling rate of 0.211×10^{12} K/s. Results from radial distribution functions (RDF) and common neighbor analysis (CNA) indicated that no crystalline structures were formed for these glassy alloys. The deformation behaviour and mechanisms of the glassy alloys at room and high temperatures and various strain rates were investigated and reported. The tensile test results showed that the yield stress decreased markedly as temperature was increased for all the alloys. The alloys exhibited superplastic behaviour for all test conditions. More importantly, by increasing the molar ratio of aluminum from 0.5 to 3.0, the yield stress and elastic modulus decreased considerably. Also, the yield stress increased with increasing the strain rate for all samples with different aluminum concentrations. Free volume content of the alloys as well as shear banding were evaluated for these alloys to aid explanation of these results.

Keywords: High-Entropy Alloys, $Al_xCrCoFeCuNi$ alloys, Tensile properties,

*Corresponding author
Email addresses: m_bahramyan@sut.ac.ir (M. Bahramyan), r_taherzadeh@sut.ac.ir (R. Taherzadeh Mousavian), dermot.brabazon@dcu.ie (D. Brabazon)
[1]Tel.: +98 919 959 1160; Fax: +98 2144412039

1. Introduction

Molecular dynamics (MD) is a simulation technique for studying the physical movements of atoms and molecules of N-body systems. In this method, the trajectories of atoms and molecules are determined by solving Newton's equations of motion. This technique is used for fundamental understanding of the deformation mechanisms in metals and alloys[1–8].

High-Entropy Alloys (HEAs) are a fascinating new class of multi-component alloys that contain more than five principal elements in equal or near equal atomic percent. Normally, the atomic fraction of each component is greater than 5 at.% and lower than 35 at.% . These alloys called HEAs by Yeh et al. and multi-component alloys by Cantor et al. [9], that have attracted attentions because of their unique composition, microstructure, and adjustable properties [10–29].

The most convenient method of fabrication of HEAs is vacuum casting and solidification, in which phase separation occurs, leading to a degradation in the mechanical properties. On the other hand, the HEAs may also undergo solidification without crystallizing, leading to an amorphous, atomistic structure. These metals are called Metallic Glasses (MGs) and they do not have dislocations as do crystalline metals, leading to relatively superior strength. [30–32].Therefore, recently, researchers focused on the formation of high entropy glassy alloys with amorphous structures. These MGs have a very high entropy of mixing and high glass forming ability (GFA) [9]. Some studies have reported the properties of these alloys [33–35]. For example, glass transition behaviour, structural relaxation and crystallization of TiZrHfNiCuAgAl, TiZrHFNiCuAl and TiZrHfNbNiCuAl MGs were investigated in detail [35]. One of the most extensively investigated HEAs with excellent mechanical properties is $Al_xCrCoFeCuNi$ [36–56], where x (the molar ratio in the alloy) ranges from 0 to 3.

To the best knowledge of authors, the tensile behaviour of AlCoCrFeCuNi alloys with an amorphous structure has not been studied at atomic scale at the room and elevated temperatures. It is very important to observe the mechanical properties of these alloys in the glassy state to understand the effect of amorphous structure and variation of the Al concentrations on the mechanical properties of such materials. Here, MD simulations are used to analyze the $Al_xCrCoFeCuNi$ alloys with glassy structure under the uniaxial tensile loading and the behaviour of these alloys at different temperature and different strain rate for various concentrations of Al.

2. Simulation Details

In MD simulations, choosing a reliable interatomic potential measure is very important to obtain reasonable results. Therefore, in this study, for describing the interatomic interaction between Al-Cr-Co-Fe-Cu-Ni, EAM (Embedded Atom Method) potential was used [57, 58]. It should be noted that based on the concept of density functional theory, this potential is non-pairwise. In the EAM potentials, the total energy E can be expressed as [57, 58]:

$$E_{pot} = \sum_{i=1}^{N} E_i = \frac{1}{2} \sum_{i,j,i\neq j}^{N} \phi_{ij}(r_{ij}) + \sum_{i} F_i(\rho_i) \tag{1}$$

where E_i is the potential energy of the atom i, ϕ_{ij} is the pair energy between atoms i and j as a function of their distance (r_{ij}) and $F_i(\rho_i)$ is the embedding energy term as a function of the local electron density (ρ_i), at the position of atom i. The local electron density can be calculated using

$$\rho_i = \sum_{j,j\neq 1}^{N} f_i(r_{ij}) \tag{2}$$

where $f_i(r_{ij})$ is the contribution of atom j at the site of atom i to the electron density. In the EAM alloy potential model, the pair potentials are defined as :

$$\phi(r) = \frac{Aexp[-\alpha(\frac{r}{r_e}) - 1]}{1 + (\frac{r}{r_e} - \kappa)^{20}} - \frac{Bexp[-\beta(\frac{r}{r_e}) - 1]}{1 + (\frac{r}{r_e} - \lambda)^{20}} \tag{3}$$

where r_e is the equilibration spacing between nearest neighbors, A, B, α and β are four adjustable parameters, and κ and λ are two additional parameters for the cutoff. The electron density function is taken with the same form as the attractive term in the pair potential with the same value of β and λ [58].

The electron density function is:

$$f(r) = \frac{f_e exp[-\beta(\frac{r}{r_e} - 1)]}{1 + (\frac{r}{r_e} - \lambda)^{20}} \tag{4}$$

The pair potential between two different species, for example a and b is then constructed as

$$\phi^{ab}(r) = \frac{1}{2}[\frac{f^b(r)}{f^a(r)}\phi^{aa}(r) + \frac{f^a(r)}{f^b(r)}\phi^{bb}(r)] \tag{5}$$

The embedding energy functions are represented by the below equations, defining the function in different electron density ranges. These equations are: [58]

$$F(\rho) = \sum_{i=0}^{3} F_{ni}(\frac{\rho}{0.85\rho_e} - 1)^i, \rho < 0.85\rho_e \tag{6}$$

$$F(\rho) = \sum_{i=0}^{3} F_i(\frac{\rho}{\rho_e} - 1)^i, 0.85\rho_e \leq \rho < 1.15\rho_e \tag{7}$$

$$F(\rho) = F_n[1 - \eta ln(\frac{\rho}{\rho_s})](\frac{\rho}{\rho_s})^\eta, \rho \geq 1.15\rho_e \tag{8}$$

where F_{ni}, F_i and F_n are tabulated constants [57–59].

The atoms of $Al_xCrCoFeCuNi$ (x= 0.5,1.5,3.0) are randomly positioned within the FCC crystal structure in the three-dimensional cell simulation with x, y and z displacement coordinates. The simulation cell size was $(72 \times 10^{-10}m) \times (72 \times 10^{-10}m) \times (180 \times 10^{-10}m)$ along x, y and z directions, which contains 80,000 atoms. The crystallographic orientation along these directions were [100], [010] and [001], respectively. Periodic boundary conditions were applied in all the three directions. Energy minimization was carried out using the conjugate gradient relaxation algorithm with the stopping tolerance for energy and force equal to 10^{-15} and $1.6 \times 10^{-24}(N)$, respectively, for relaxation of the randomized HEAs configuration. The relaxed structure was initialized at room

temperature (300°K) under an isothermal-isobaric or NPT (constant number of particle (N), constant pressure (P) and constant temperature (T)) ensemble at a pressure of 0 MPa for 30×10^{-12} s. The system was then heated at a heating rate of 0.211×10^{12} K/s to 2200°K to melt the alloy. After that, the system was equilibrated at 2200°K for 45×10^{-12} s. This step was followed by a quick quenching with a cooling rate of 0.211×10^{12} K/s to 300°K and relaxed at 300°K under an isothermal-isobaric ensemble at a pressure of 0 MPa for 45×10^{-12} s. Rapid quenching was implemented to ensure that the HEA-MGs were created. Finally, to ensure that an metastabled structure was obtained, the entire system was simulated and relaxed using Nose/Hoover temperature thermostat (NVT or canonical ensemble) and followed by microcanonical (NVE) ensemble in the absence of thermodynamic constraints.

The temperatures examined in the prepared isobaric-isothermal ensemble in the HEA model were 300°K,700°K,1000°K and 1300°K. The Verlet algorithm was used for integrating the equation of motion with a time step of 2×10^{-15} s. Before applying the tensile loading, the model was relaxed to get an metastable state at the desired temperature. Uniaxial tensile loading along the z direction was then applied. The large-scale atomic/molecular massively parallel simulator (LAMMPS) [60] was used for MD simulations and trajectories of atoms were studied using visual molecular dynamics (VMD) [61].

3. Results and Discussion

In order to study the atomic structure of the prepared alloys after solidification, pair correlation functions, g(r) of the $Al_{0.5}$CrCoFeCuNi at 2200°K and 300°K were calculated and are shown in the Fig. 1. As can be seen in this Fig. 1, for both the temperatures, an amorphous structure was obtained while in the liquid phase, the corresponding peaks were broader with a lower intensity. Therefore, the atomic order of the solidified alloys was slightly higher than that of the melt. Fig. 2 shows g(r) of $Al_{0.5}$CrCoFeCuNi at 300°K for all of the atom pairs before the tensile loading. It should be noted that for the higher

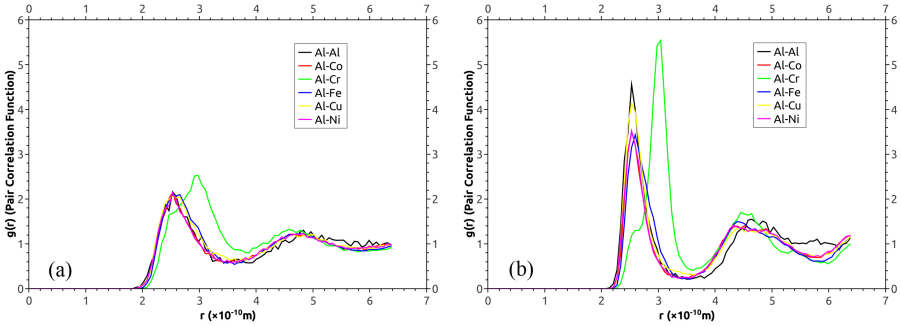

Fig. 1: Radial Distribution functions of Al pairs for $Al_{0.5}$CrCoFeCuNi at a) 2200°K and b) 300°K.

temperatures (700, 1000 and 1300°K), the results of the g(r) were almost the same. It can be seen from this Fig. 2 that there was strong affinity between like pairs (e.g. Al-Al, Cr-Cr, Co-Co) and unlike pairs (e.g. Al-Cr, Al-Co). Also, the distribution of each element was shown to be uniform from the HEA model as shown in Fig. 3. On the other hand, the CNA (Common Neighbor Analysis) [62, 63] results of each atoms showed that there were no FCC, BCC, HCP (Hexagonal Close-Packed) and icosahedral structures in the samples. From the topological disorder and chemical disorder results, these alloy compositions can be classified as HEA-MGs.

The HEA model $Al_{0.5}$CrCoFeCuNi at 300°K is shown in Fig. 4. The sequence of the stress-strain curve at the strain rate equal to $10^{10}s^{-1}$ can be observed in this Fig. 4 The stress was increased with increasing the strain at the initial stage of deformation, just as in single-crystal materials. After that, plastic deformation started and the deformation underwent significant changes indicating superplastic behaviour of the alloy.

Plastic deformation of MGs at low temperatures is characterized by localization of flow into narrow regions within the volume of the material. These regions are often referred as shear bands (SBs), which normally determine the mechanical properties of MGs, especially their ductility and toughness. Pre-

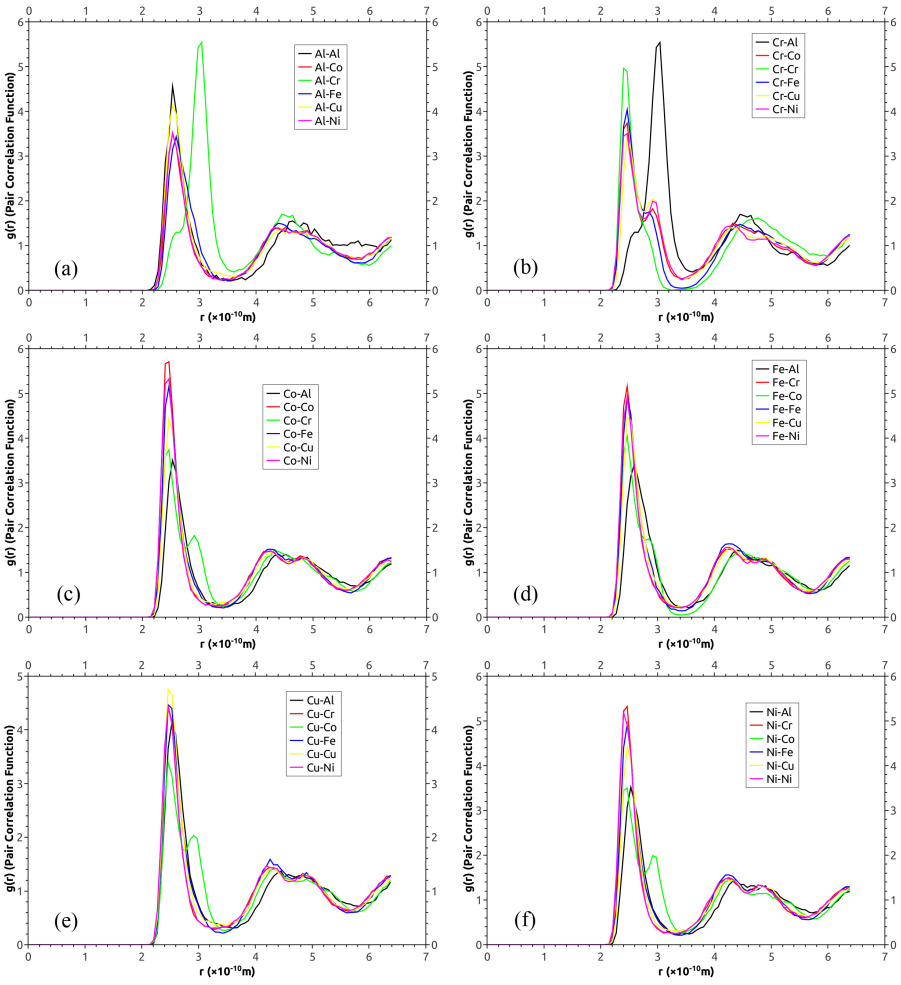

Fig. 2: Radial Distribution functions of all atom pairs for $Al_{0.5}CrCoFeCuNi$ at 300°K. The pair correlations of like pairs (e.g.,Al-Al) and unlike pairs (e.g., Al-Cr) indicate strong affinity among the like pairs and unlike pairs.

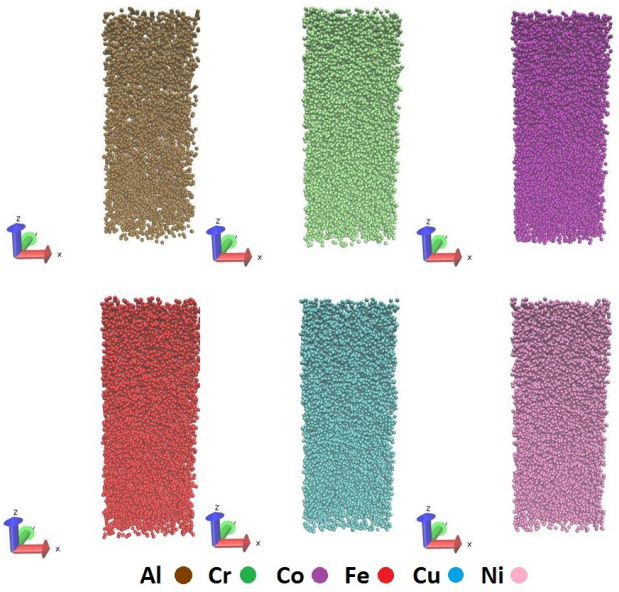

Fig. 3: Distribution of each element in $Al_{0.5}CrCoFeCuNi$ at 300°K.

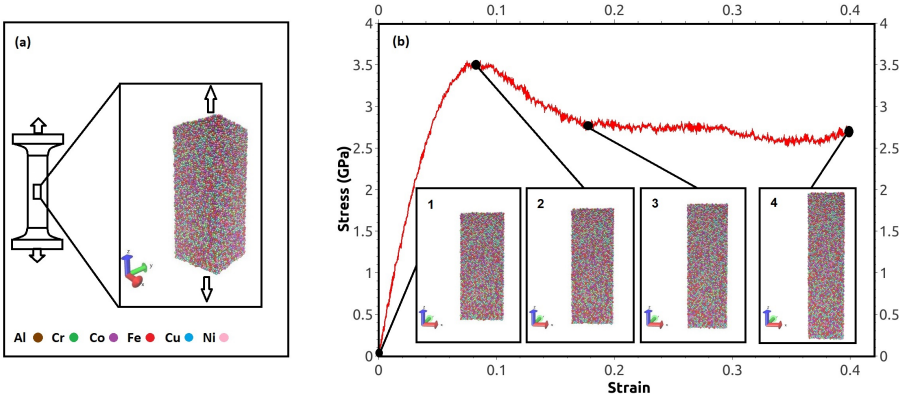

Fig. 4: (a) Schematic of conventional tensile specimen, and schematic of the atomic $Al_{0.5}CrCoFeCuNi$ HEA sample for MD simulations under the tensile loading, in which the arrows indicate the loading directions, (b) the stress-strain curve of tensile behaviour of $Al_{0.5}CrCoFeCuNi$ at 300°K at the strain rate equal to $10^{10}s^{-1}$ with atomic snapshots at different stages.

Table 1: Free volume ($\times 10^{-27}$m^3) in different molar ratio of Al in $Al_xCrCoFeCuNi$ and equal number of atoms (80000 atoms) with different strain rate at 300°K.

x value in $Al_xCrCoFeCuNi$	0.5	1.5	3.0
Strain =0.0	302.4	307	317.8
Strain =0.2, Strain Rate = 10^9	309.7	314.3	325.7
Strain =0.08, Strain Rate = 10^{10}	313.8	318.6	329.6
Strain =0.2, Strain Rate = 10^{10}	312.8	317.8	329.1
Strain =0.2, Strain Rate = 10^{11}	325.3	330.5	341.4

vious studies have indicated that the presence of SBs in MGs can lead to the formation of a higher free volume, causing a reduction in the density of MGs. This high free volume values can lead to the strain softening during plastic deformation. In addition, their low density can enhance the diffusion rate within the SBs [64]. Therefore, the free volume of the samples for the first, second (when overshooting occurs), and third stages were calculated using Voronoi tessellation technique [65, 66] (see Table 1). Deformation stages of $Al_{0.5}CrCoFeCuNi$ are shown in Fig. 4 (b). The atomic radiuses of the elements used for this calculation are given in Table 2. These results indicate that by increasing the aluminum content at 300°K, a higher free volume was obtained for the alloys before starting the tensile test. Therefore, a higher strain softening and diffusion rate can be expected for the alloys containing a higher concentration of aluminum. In addition, it was found that the free volume in the third stage in the Fig. 4 (b) was 10^{-26}m^3 higher than that in the first stage in the $Al_{0.5}CrCoFeCuNi$ sample at 300°K. This increase might represent the formation of SBs [64] during plastic deformation.

The tensile behaviour of all the samples at the strain rate of 10^{10}s^{-1} is shown in Fig. 5 (a, b, c, and d). As can be seen, at each temperature, the value of yield stress was decreased by increasing the Al concentration. Also, at lower temperatures, a peak in the stress occurred before start of the plastic deformation. This

Table 2: Atomic radiuses of each elements used in interatomic potential

Elements	Al	Cr	Co	Fe	Cu	Ni
Atomic radius ($\times 10^{-10}$m)	1.43	1.24	1.25	1.24	1.27	1.24

overshoot behaviour of stress can be explained by considering the interaction between shear transformation zones (STZs) and free volume dynamics [64]. As mentioned, based on formation of this overshoot, the free volume at the second stage was calculated. The calculated free volume at the second stage (strain = 0.08) at 300°K for all aluminum concentrations showed that the amount of free volume was increased at the peak of these stress-strain curves, see Table 1. Dynamic activation of STZs and the STZ-mediated free volume dynamics were utilized to obtain the amorphous plastic types. Cheng et al. [67] illustrated that the shear stress for initial yielding expressed the fundamental resistance to flow initiation of the amorphous HEAs, while the stress in the steady-state flow area, shows the shear resistance of the fresh glass structure. In summary, based on the results of Table 1, a higher free volume in the first stage (strain = 0.0) promotes structural softening, and hence causes easier interaction between STZs. In addition, Figs. 5 (e) and (f) showed that the strength of the alloys decreased by increasing the temperature. Some studies have reported that in HEAs that have chemical clustering or ordering behaviour, there is a reasonably good mechanical strength at elevated temperatures compared to ambient temperature[68], however, the obtained results of this study showed that in HEAs with an amorphous structure, the tensile strength has a considerable decreasing trend by increasing the temperature (see Fig. 5 (e)). Furthermore, the type of deformation seems to be different at the higher temperatures versus the lower temperatures. Jafari-zadeh et al. [69] showed that in the metallic glasses, at low temperature, a single shear band is activated while for intermediate and high temperatures multiple shear-banding and homogeneous plastic flow are activated, respectively. As a result, they are expected to cause a reduc-

Table 3: Calculated free volume of the $Al_{0.5}CrCoFeCuNi$ sample at different temperatures.

Temperature (°K)	300	700	1000	1300
Free volume ($\times 10^{-27} m^3$)	302	319	334	354

tion in the yield stress by increasing the temperature. In addition, Literature reported that there is a relationship between the glass transition temperature (T_g) and deformation mechanisms for MGs. Based on the deformation map of MGs [70], homogenous deformations occurs when the actual temperature is almost equal or higher than the glass transition temperature. Therefore, the T_g of the $Al_{0.5}CrCoFeCuNi$ was determined during the quenching process by analyzing the changes of average potential energy for each atom as a function of temperature. As can be seen in the Fig. 6. During the cooling process, by decreasing the temperature, the potential energy of the system was decreased and T_g was evaluated from the deviation of the potential energy from its linear relationship with temperature [71, 72]. Therefore, the estimated T_g was about 800°K, indicating that the tensile behaviour of these alloys and the mechanism of deformation is different after this range of temperature.

In order to examine the differences between deformation mechanisms at the high and low temperatures, another simulation was performed. In this simulation, the periodic boundary of the lateral faces was fixed (x and y). The results are shown in the Fig. 7. The deformation behaviour of the samples at the two temperatures for $\varepsilon = 1.0$ were found to be different. At the low temperature (300 °K), necking occurred which is resultant from localized deformation, while at the higher temperature (1300 °K) no necking was observed which is resultant from more homogeneous deformation. In addition, free volumes of the samples at each temperature (Table 3) showed that by increasing the temperature, the free volume was increased, which caused a higher tensile ductility. Based on the deformation map of MGs, homogeneous deformations occurred at these high temperatures [70] at the strain rate equal to $10^{10} s^{-1}$.

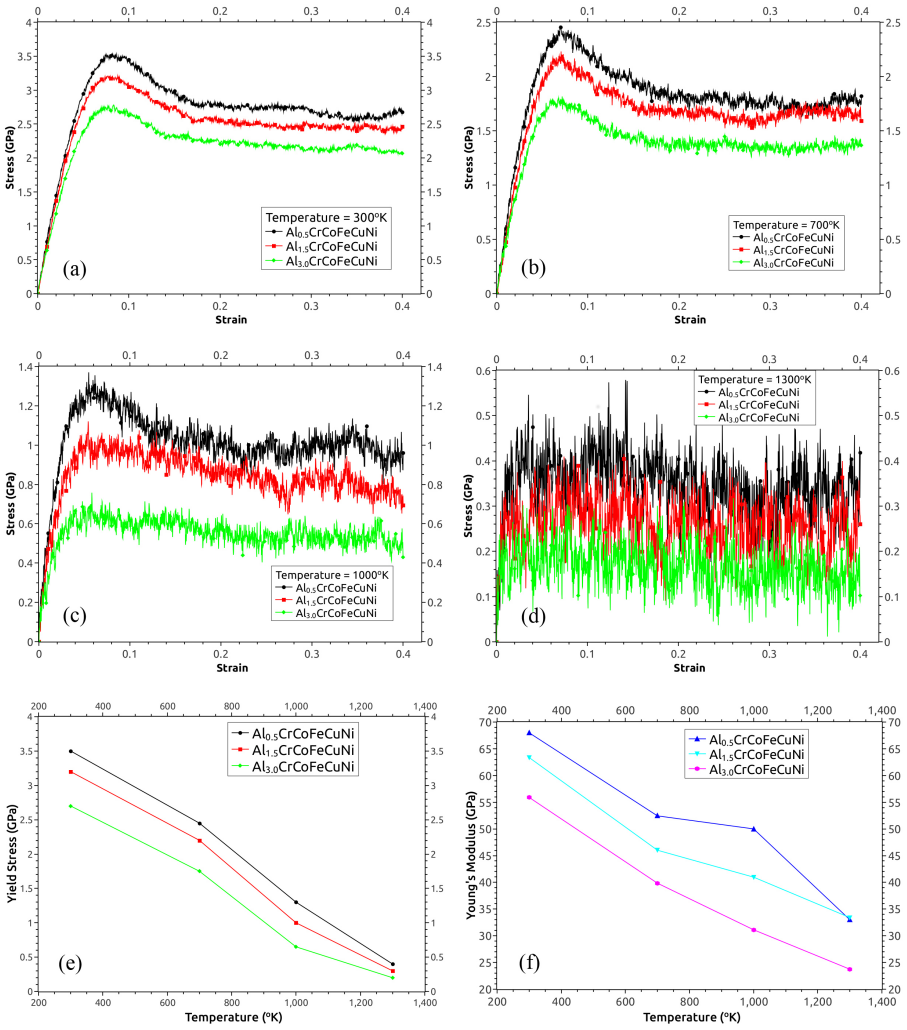

Fig. 5: Stress-Strain curve of HEA model at the strain rate equal to $10^{10}s^{-1}$ with different Al concentration at different temperature (a)300°K, (b)700°K, (c)1000°K, (d)1300°K, (e) Yielding Stress at different temperatures and different Al concentrations, (f) Young's Modulus at different temperatures and different Al concentrations.

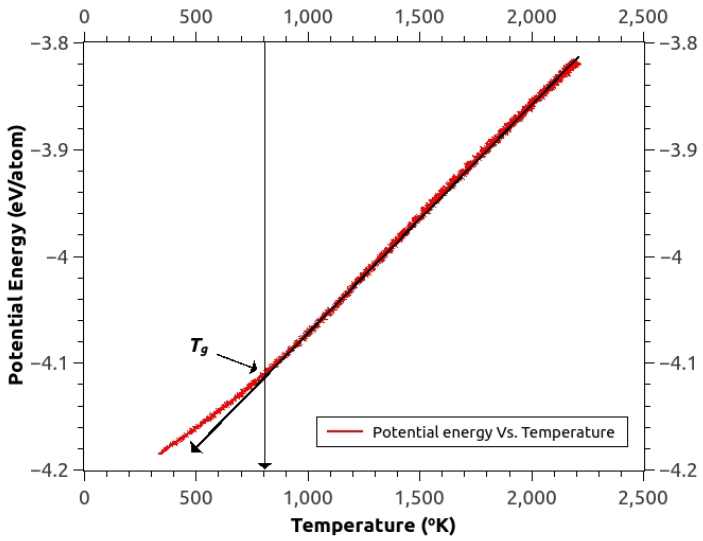

Fig. 6: Potential energy per atom as a function of temperature during the simulated quenching process to estimate the value of T_g in $Al_{0.5}CrCoFeCuNi$.

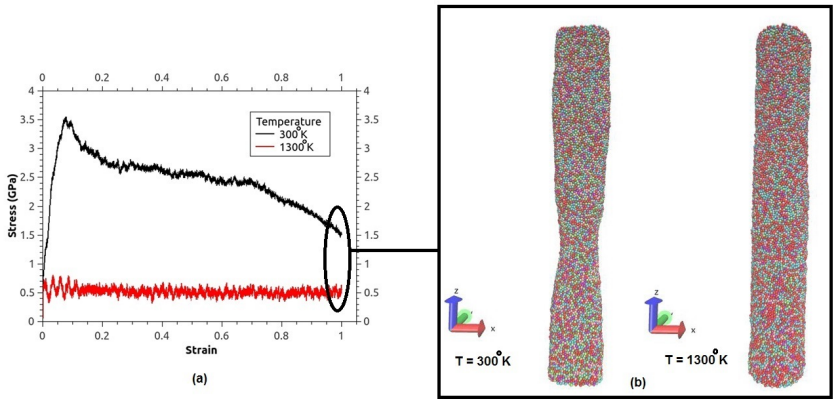

Fig. 7: a) Stress-Strain curve of $Al_{0.5}CrCoFeCuNi$ sample at the strain rate equal to $10^{10}s^{-1}$ at 300 $°K$ and 1300 $°K$ b) atomic snapshots during tensile test in $\varepsilon = 1.0$

In order to study the effect of strain rate on the tensile behaviour, some simulations with different strain rates were performed. Stress-Strain curves of the samples with different concentrations of aluminum and different strain rates are shown in Fig. 8. As can be seen in this Fig. 8, by increasing the strain rate, the yield stress was increased at 300°K and 1300°K for different aluminum concentrations. In addition, the free volume values of samples in the third stage of deformation during plastic deformation in strain equal to 0.2 were calculated. The results in $Al_{0.5}$CrCoFeCuNi are showed in Table 1 and 4 for 300°K and 1300°K, respectively. As can be seen, the free volume of all samples was increased with increasing the strain rate. However, at 1300°K at the strain rate equal to 10^9, the value of free volume in the first and third stages is almost the same. For the higher strain rates, the increment in amount of free volume is smaller than 300°K. This difference could be due to the different deformation mechanisms in these two temperatures. There is direct relationship between strain rate and free volume as reported in the study of Heggen at al. [73]. Therefore, by increasing the strain rate, a higher free volume will be obtained. However, at a higher strain rate, the required time for diffusion of atoms and rearrangement of free volume will be considerably decreased, and therefore the effective free volume that aid the mobility of atoms during deformation will be decreased [74]. Thus, a higher strength will be obtained and the motion of atoms will be difficult during deformation. Fig. 9 shows a change in the yield stress by increasing the strain rate. As can be seen, at the higher strain rates, a higher stress seems to be needed to start the plastic deformation at 300°K and 1300°K.

4. Conclusions

The tensile behaviour of glassy Al_xCrCoFeCuNi HEAs from 300°K to 1300°K were determined in this study. For this purpose, the alloys were cooled at a high rate to prepare amorphous structures. From the simulation results, the following conclusions can be drawn:

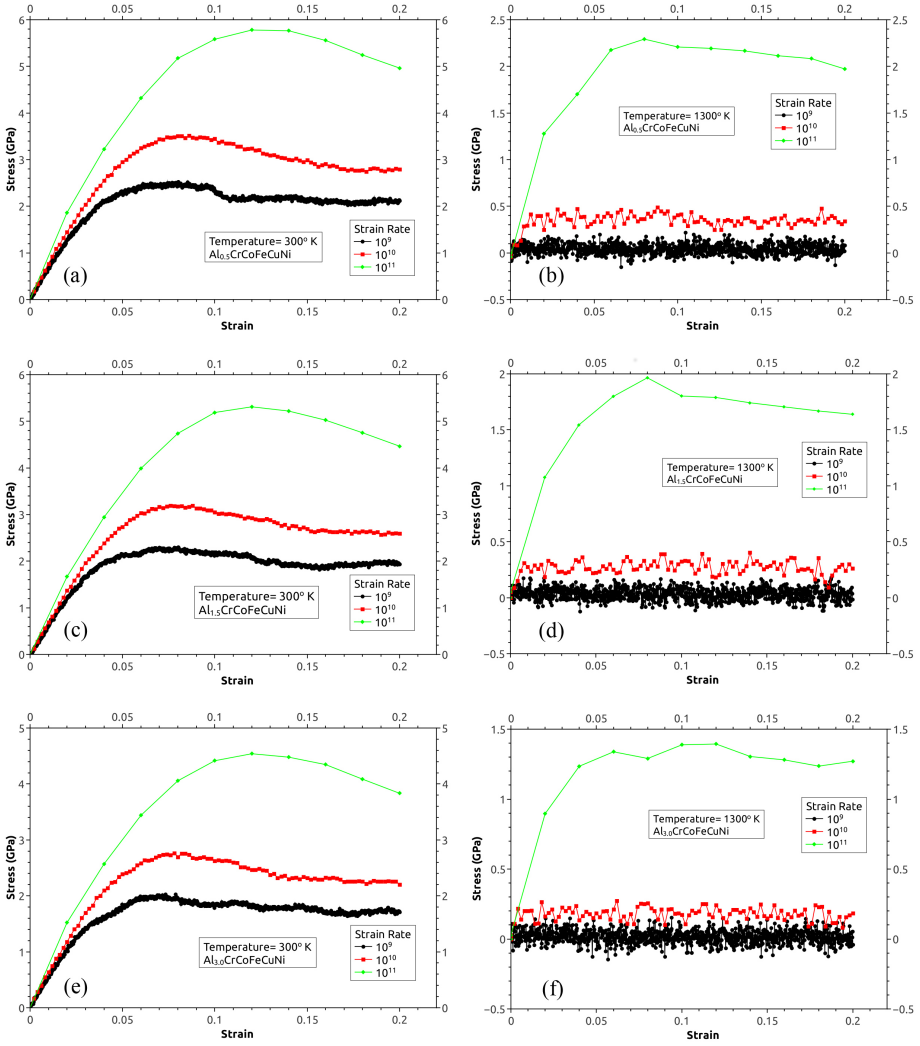

Fig. 8: Stress-Strain curves of $Al_xCrCoFeCuNi$ samples at two different temperatures and different strain rates.

Table 4: Free volume ($\times 10^{-27} m^3$) in different molar ratio of Al in $Al_xCrCoFeCuNi$ and equal number of atoms (80000 atoms) with different strain rate at 1300°K.

x value in $Al_xCrCoFeCuNi$	0.5	1.5	3.0
Strain =0.0	354.1	360.1	375.8
Strain =0.2, Strain Rate = 10^9	353.8	359.6	375.2
Strain =0.2, Strain Rate = 10^{10}	355.1	361.6	377
Strain =0.2 , Strain Rate = 10^{11}	366.1	371.9	386.6

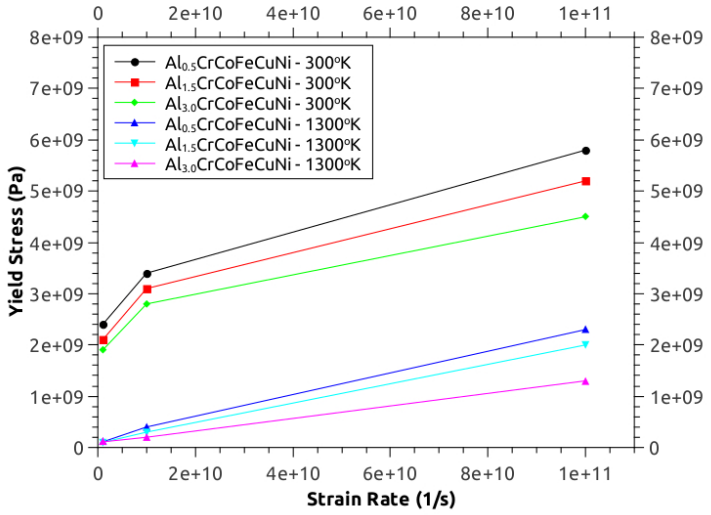

Fig. 9: Strain rate versus Yield stress in $Al_xCrCoFeCuNi$ at 300°K and 1300°K.

1. RDF and CNA results indicated that no crystalline structures were formed for the alloys; although, the short range atomic order of the solidified alloys was higher than that of the melt.
2. The tensile yield stress of all the alloys decreased considerably by increasing of the temperature. In addition, it was found that all of the alloys exhibited superplastic behaviour.
3. It was found that by increasing the amount of molar ratio of aluminum from 0.5 to 3.0, the yield stress and elastic modulus were considerably decreased. This can be understood after determination of the free volume content of the alloys. A higher free volume content was formed for the alloys with higher concentrations of aluminum, leading to the activation of shear bands and hence the promotion of deformation.
4. Although, at the higher rate of strain, a higher free volume was obtained, however, the yield stress of all the samples was increased by increasing the strain rate due to lack of required time for the diffusion and rearrangement of atoms that caused a lower effective free volume.

References

[1] G. Bomarito, Y. Lin, D. Warner, An atomistic modeling survey of the shear strength of twist grain boundaries in aluminum, Scripta Materialia 101 (2015) 72–75. doi:10.1016/j.scriptamat.2015.01.022.

[2] R. Cao, C. Deng, The ultra-small strongest grain size in nanocrystalline Ni nanowires, Scripta Materialia 94 (2015) 9–12. doi:10.1016/j.scriptamat.2014.09.002.

[3] Y. N. Osetsky, D. J. Bacon, Atomic-scale mechanisms of void hardening in bcc and fcc metals, Philosophical magazine 90 (7-8) (2010) 945–961. doi:10.1080/14786430903164580.

[4] Y. N. Osetsky, D. J. Bacon, An atomic-level model for studying the dynamics of edge dislocations in metals, Modelling and simulation in materials

science and engineering 11 (4) (2003) 427. doi:10.1088/0965-0393/11/4/302.

[5] R. Veiga, H. Goldenstein, M. Perez, C. Becquart, Monte Carlo and molecular dynamics simulations of screw dislocation locking by Cottrell atmospheres in low carbon Fe–C alloys, Scripta Materialia 108 (2015) 19–22. doi:10.1016/j.scriptamat.2015.06.012.

[6] M. Mendelev, M. Kramer, R. Ott, D. Sordelet, Molecular dynamics simulation of diffusion in supercooled Cu–Zr alloys, Philosophical Magazine 89 (2) (2009) 109–126. doi:10.1080/14786430802570648.

[7] J. Davoodi, S. Dadashi, M. Yarifard, Molecular dynamics simulations of the melting of Al–Ni nanowires, Philosophical Magazine 96 (22) (2016) 2300–2310. doi:10.1080/14786435.2016.1198053.

[8] M. Bahramyan, R. T. Mousavian, D. Brabazon, Molecular dynamic simulation of edge dislocation-void interaction in pure Al and Al-Mg alloy, Materials Science and Engineering: A 674 (2016) 82–90. doi:10.1016/j.msea.2016.07.121.

[9] Y. Zhang, T. T. Zuo, Z. Tang, M. C. Gao, K. A. Dahmen, P. K. Liaw, Z. P. Lu, Microstructures and properties of high-entropy alloys, Progress in Materials Science 61 (2014) 1–93. doi:10.1016/j.pmatsci.2013.10.001.

[10] L. Patriarca, A. Ojha, H. Sehitoglu, Y. Chumlyakov, Slip nucleation in single crystal FeNiCoCrMn high entropy alloy, Scripta Materialia 112 (2016) 54–57. doi:10.1016/j.scriptamat.2015.09.009.

[11] J.-C. Huang, Evaluation of Tribological Behavior of Al-Co-Cr-Fe-Ni High Entropy Alloy Using Molecular Dynamics Simulation, Scanning 34 (5) (2012) 325–331. doi:10.1002/sca.21006.

[12] E.-W. Huang, D. Yu, J.-W. Yeh, C. Lee, K. An, S.-Y. Tu, A study of lattice elasticity from low entropy metals to medium and high entropy

alloys, Scripta Materialia 101 (2015) 32–35. doi:10.1016/j.scriptamat.2015.01.011.

[13] T. Smith, M. Hooshmand, B. Esser, F. Otto, D. McComb, E. George, M. Ghazisaeidi, M. Mills, Atomic-scale characterization and modeling of 60° dislocations in a high-entropy alloy, Acta Materialia 110 (2016) 352–363. doi:10.1016/j.actamat.2016.03.045.

[14] G. Anand, R. Goodall, C. L. Freeman, Role of configurational entropy in body-centred cubic or face-centred cubic phase formation in high entropy alloys, Scripta Materialia 124 (2016) 90–94. doi:10.1016/j.scriptamat.2016.07.001.

[15] Z. Wang, M. Gao, S. Ma, H. Yang, Z. Wang, M. Ziomek-Moroz, J. Qiao, Effect of cold rolling on the microstructure and mechanical properties of $Al_{0.25}CoCrFe_{1.25}Ni_{1.25}$ high-entropy alloy, Materials Science and Engineering: A 645 (2015) 163–169. doi:10.1016/j.msea.2015.07.088.

[16] Z. Tang, O. N. Senkov, C. M. Parish, C. Zhang, F. Zhang, L. J. Santodonato, G. Wang, G. Zhao, F. Yang, P. K. Liaw, Tensile ductility of an AlCoCrFeNi multi-phase high-entropy alloy through hot isostatic pressing (HIP) and homogenization, Materials Science and Engineering: A 647 (2015) 229–240. doi:10.1016/j.msea.2015.08.078.

[17] C.-M. Lin, H.-L. Tsai, Evolution of microstructure, hardness, and corrosion properties of high-entropy $Al_{0.5}CoCrFeNi$ alloy, Intermetallics 19 (3) (2011) 288–294. doi:10.1016/j.intermet.2010.10.008.

[18] A. Munitz, S. Salhov, S. Hayun, N. Frage, Heat treatment impacts the micro-structure and mechanical properties of AlCoCrFeNi high entropy alloy, Journal of Alloys and Compounds 683 (2016) 221–230. doi:10.1016/j.jallcom.2016.05.034.

[19] J. Dabrowa, W. Kucza, G. Cieslak, T. Kulik, M. Danielewski, J.-W. Yeh, Interdiffusion in the FCC-structured Al-Co-Cr-Fe-Ni high entropy alloys:

Experimental studies and numerical simulations, Journal of Alloys and Compounds 674 (2016) 455–462. doi:10.1016/j.jallcom.2016.03.046.

[20] J. J. Licavoli, M. C. Gao, J. S. Sears, P. D. Jablonski, J. A. Hawk, Microstructure and Mechanical Behavior of High-Entropy Alloys, Journal of Materials Engineering and Performance 24 (10) (2015) 3685–3698. doi:10.1007/s11665-015-1679-7.

[21] B. Gludovatz, A. Hohenwarter, D. Catoor, E. H. Chang, E. P. George, R. O. Ritchie, A fracture-resistant high-entropy alloy for cryogenic applications, Science 345 (6201) (2014) 1153–1158. doi:10.1126/science.1254581.

[22] Y. Zou, S. Maiti, W. Steurer, R. Spolenak, Size-dependent plasticity in an $Nb_{25}Mo_{25}Ta_{25}W_{25}$ refractory high-entropy alloy, Acta Materialia 65 (2014) 85–97. doi:10.1016/j.actamat.2013.11.049.

[23] L. Anmin, X. Zhang, Thermodynamic analysis of the simple microstructure of AlCrFeNiCu high-entropy alloy with multi-principal elements, Acta Metallurgica Sinica (English Letters) 22 (3) (2009) 219–224. doi:10.1016/S1006-7191(08)60092-7.

[24] S. Ma, Z. Jiao, J. Qiao, H. Yang, Y. Zhang, Z. Wang, Strain rate effects on the dynamic mechanical properties of the $AlCrCuFeNi_2$ high-entropy alloy, Materials Science and Engineering: A 649 (2016) 35–38. doi:10.1016/j.msea.2015.09.089.

[25] C. C. Tasan, Y. Deng, K. G. Pradeep, M. Yao, H. Springer, D. Raabe, Composition dependence of phase stability, deformation mechanisms, and mechanical properties of the CoCrFeMnNi high-entropy alloy system, Jom 66 (10) (2014) 1993–2001. doi:10.1007/s11837-014-1133-6.

[26] T.-T. Shun, Y.-C. Du, Age hardening of the $Al_{0.3}CoCrFeNiC_{0.1}$ high entropy alloy, Journal of alloys and compounds 478 (1) (2009) 269–272. doi:10.1016/j.jallcom.2008.12.014.

[27] P. Jinhong, P. Ye, Z. Hui, Z. Lu, Microstructure and properties of $AlCrFeCuNi_x(0.6 \leq x \leq 1.4)$ high-entropy alloys, Materials Science and Engineering: A 534 (2012) 228–233. doi:10.1016/j.msea.2011.11.063.

[28] S. G. Ma, Z. D. Chen, Y. Zhang, Evolution of microstructures and properties of the $Al_xCrCuFeNi_2$ high-entropy alloys, in: Materials Science Forum, Vol. 745, Trans Tech Publ, 2013, pp. 706–714. doi:10.4028/www.scientific.net/MSF.745-746.706.

[29] I. Wani, T. Bhattacharjee, S. Sheikh, Y. Lu, S. Chatterjee, P. Bhattacharjee, S. Guo, N. Tsuji, Ultrafine-grained $AlCoCrFeNi_{2.1}$ eutectic high-entropy alloy, Materials Research Letters 4 (3) (2016) 174–179. doi:10.1080/21663831.2016.1160451.

[30] M. Telford, The case for bulk metallic glass, Materials today 7 (3) (2004) 36–43. doi:10.1016/S1369-7021(04)00124-5.

[31] C. Suryanarayana, A. Inoue, Bulk metallic glasses, CRC Press, 2010.

[32] D. Rodney, A. Tanguy, D. Vandembroucq, Modeling the mechanics of amorphous solids at different length scale and time scale, Modelling and Simulation in Materials Science and Engineering 19 (8) (2011) 083001. doi:10.1088/0965-0393/19/8/083001.

[33] A. Takeuchi, M. C. Gao, J. Qiao, M. Widom, High-Entropy Metallic Glasses, in: High-Entropy Alloys, Springer, 2016, pp. 445–468.

[34] W. Wang, High-entropy metallic glasses, Jom 66 (10) (2014) 2067–2077. doi:10.1007/s11837-014-1002-3.

[35] K. Kim, P. Warren, B. Cantor, Structural relaxation and glass transition behavior of novel $(Ti_{33}Zr_{33}Hf_{33})_{50}(Ni_{50}Cu_{50})_{40}Al_{10}$ alloy developed by equiatomic substitution, Journal of Non-Crystalline Solids 353 (32) (2007) 3338–3341. doi:10.1016/j.jnoncrysol.2007.05.081.

[36] L. J. Santodonato, Y. Zhang, M. Feygenson, C. M. Parish, M. C. Gao, R. J. Weber, J. C. Neuefeind, Z. Tang, P. K. Liaw, Deviation from high-entropy configurations in the atomic distributions of a multi-principal-element alloy, Nature communications 6. doi:10.1038/ncomms6964.

[37] T. Chung-Jin, C. Min-Rui, S.-K. Chen, J.-W. Yeh, et al., Mechanical Performance of the Al_xCoCrCuFeNi High-Entropy Alloy System with Multi-principal Elements, Metallurgical and Materials Transactions 36 (5) (2005) 1263. doi:10.1007/s11661-005-0218-9.

[38] C.-W. Tsai, M.-H. Tsai, J.-W. Yeh, C.-C. Yang, Effect of temperature on mechanical properties of $Al_{0.5}$CoCrCuFeNi wrought alloy, Journal of Alloys and Compounds 490 (1) (2010) 160–165. doi:10.1016/j.jallcom.2009.10.088.

[39] A. Manzoni, H. Daoud, S. Mondal, S. Van Smaalen, R. Völkl, U. Glatzel, N. Wanderka, Investigation of phases in $Al_{23}Co_{15}Cr_{23}Cu_8Fe_{15}Ni_{16}$ and $Al_8Co_{17}Cr_{17}Cu_8Fe_{17}Ni_{33}$ high entropy alloys and comparison with equilibrium phases predicted by Thermo-Calc, Journal of Alloys and Compounds 552 (2013) 430–436. doi:10.1016/j.jallcom.2012.11.074.

[40] D. Shaysultanov, N. Stepanov, A. Kuznetsov, G. Salishchev, O. Senkov, Phase composition and superplastic behavior of a wrought AlCoCrCuFeNi high-entropy alloy, Jom 65 (12) (2013) 1815–1828. doi:10.1007/s11837-013-0754-5.

[41] L. Xie, P. Brault, A.-L. Thomann, J.-M. Bauchire, AlCoCrCuFeNi high entropy alloy cluster growth and annealing on silicon: A classical molecular dynamics simulation study, Applied Surface Science 285 (2013) 810–816. doi:10.1016/j.apsusc.2013.08.133.

[42] L. Xie, P. Brault, A.-L. Thomann, X. Yang, Y. Zhang, G. Shang, Molecular dynamics simulation of Al–Co–Cr–Cu–Fe–Ni high entropy alloy thin film growth, Intermetallics 68 (2016) 78–86. doi:10.1016/j.intermet.2015.09.008.

[43] C.-J. Tong, Y.-L. Chen, J.-W. Yeh, S.-J. Lin, S.-K. Chen, T.-T. Shun, C.-H. Tsau, S.-Y. Chang, Microstructure characterization of Al_xCoCrCuFeNi high-entropy alloy system with multiprincipal elements, Metallurgical and Materials Transactions A 36 (4) (2005) 881–893. doi:10.1007/s11661-005-0283-0.

[44] M.-H. Tsai, J.-W. Yeh, High-entropy alloys: a critical review, Materials Research Letters 2 (3) (2014) 107–123. doi:10.1080/21663831.2014.912690.

[45] C. Yu, X. Xu, M. Chen, C. Liu, Atomistic mechanism of nano-scale phase separation in fcc-based high entropy alloys, Journal of Alloys and Compounds 663 (2016) 340–344. doi:10.1016/j.jallcom.2015.12.004.

[46] X. Xu, P. Liu, S. Guo, A. Hirata, T. Fujita, T. Nieh, C. Liu, M. Chen, Nanoscale phase separation in a fcc-based $CoCrCuFeNiAl_{0.5}$ high-entropy alloy, Acta Materialia 84 (2015) 145–152. doi:10.1016/j.actamat.2014.10.033.

[47] F. Wang, Y. Zhang, G. Chen, H. A. Davies, Tensile and compressive mechanical behavior of a $CoCrCuFeNiAl_{0.5}$ high entropy alloy, International Journal of Modern Physics B 23 (06n07) (2009) 1254–1259. doi:10.1142/S0217979209060774.

[48] S. Singh, N. Wanderka, B. Murty, U. Glatzel, J. Banhart, Decomposition in multi-component AlCoCrCuFeNi high-entropy alloy, Acta Materialia 59 (1) (2011) 182–190. doi:10.1016/j.actamat.2010.09.023.

[49] E. Pickering, H. Stone, N. Jones, Fine-scale precipitation in the high-entropy alloy $Al_{0.5}$CrFeCoNiCu, Materials Science and Engineering: A 645 (2015) 65–71. doi:10.1016/j.msea.2015.08.010.

[50] V. Nadutov, S. Y. Makarenko, P. Y. Volosevich, Effect of aluminum on fine structure and distribution of chemical elements in high-entropy alloys

Al_xFeNiCoCuCr, The Physics of Metals and Metallography 116 (5) (2015) 439–444. doi:10.1134/S0031918X15030096.

[51] J.-M. Wu, S.-J. Lin, J.-W. Yeh, S.-K. Chen, Y.-S. Huang, H.-C. Chen, Adhesive wear behavior of Al_xCoCrCuFeNi high-entropy alloys as a function of aluminum content, Wear 261 (5) (2006) 513–519. doi:10.1016/j.wear.2005.12.008.

[52] U. Roy, H. Roy, H. Daoud, U. Glatzel, K. Ray, Fracture toughness and fracture micromechanism in a cast AlCoCrCuFeNi high entropy alloy system, Materials Letters 132 (2014) 186–189. doi:10.1016/j.matlet.2014.06.067.

[53] M. A. Hemphill, T. Yuan, G. Wang, J. Yeh, C. Tsai, A. Chuang, P. Liaw, Fatigue behavior of $Al_{0.5}$CoCrCuFeNi high entropy alloys, Acta Materialia 60 (16) (2012) 5723–5734. doi:10.1016/j.actamat.2012.06.046.

[54] C.-W. Tsai, Y.-L. Chen, M.-H. Tsai, J.-W. Yeh, T.-T. Shun, S.-K. Chen, Deformation and annealing behaviors of high-entropy alloy $Al_{0.5}$CoCrCuFeNi, Journal of Alloys and compounds 486 (1) (2009) 427–435. doi:10.1016/j.jallcom.2009.06.182.

[55] S. Guo, C. Ng, J. Lu, C. Liu, Effect of valence electron concentration on stability of fcc or bcc phase in high entropy alloys, Journal of applied physics 109 (10) (2011) 103505. doi:10.1063/1.3587228.

[56] A. Kuznetsov, D. Shaysultanov, N. Stepanov, G. Salishchev, O. Senkov, Tensile properties of an AlCrCuNiFeCo high-entropy alloy in as-cast and wrought conditions, Materials Science and Engineering: A 533 (2012) 107–118. doi:10.1016/j.msea.2011.11.045.

[57] M. S. Daw, S. M. Foiles, M. I. Baskes, The embedded-atom method: a review of theory and applications, Materials Science Reports 9 (7) (1993) 251–310. doi:10.1016/0920-2307(93)90001-U.

[58] X. Zhou, R. Johnson, H. Wadley, Misfit-energy-increasing dislocations in vapor-deposited CoFe/NiFe multilayers, Physical Review B 69 (14) (2004) 144113. doi:10.1103/PhysRevB.69.144113.

[59] Z. Lin, R. A. Johnson, L. V. Zhigilei, Computational study of the generation of crystal defects in a bcc metal target irradiated by short laser pulses, Physical Review B 77 (21) (2008) 214108. doi:10.1103/PhysRevB.77.214108.

[60] S. Plimpton, Fast parallel algorithms for short-range molecular dynamics, Journal of computational physics 117 (1) (1995) 1–19. doi:10.1006/jcph.1995.1039.

[61] W. Humphrey, A. Dalke, K. Schulten, VMD: visual molecular dynamics, Journal of molecular graphics 14 (1) (1996) 33–38. doi:10.1016/0263-7855(96)00018-5.

[62] D. Faken, H. Jónsson, Systematic analysis of local atomic structure combined with 3D computer graphics, Computational Materials Science 2 (2) (1994) 279–286. doi:10.1016/0927-0256(94)90109-0.

[63] H. Tsuzuki, P. S. Branicio, J. P. Rino, Structural characterization of deformed crystals by analysis of common atomic neighborhood, Computer physics communications 177 (6) (2007) 518–523. doi:10.1016/j.cpc.2007.05.018.

[64] C. Zhong, H. Zhang, Q. Cao, X. Wang, D. Zhang, U. Ramamurty, J. Jiang, Deformation behavior of metallic glasses with shear band like atomic structure: a molecular dynamics study, Scientific Reports 6. doi:10.1038/srep30935.

[65] W. Brostow, J.-P. Dussault, B. L. Fox, Construction of Voronoi polyhedra, Journal of Computational Physics 29 (1) (1978) 81–92. doi:10.1016/0021-9991(78)90110-9.

[66] M. Tanemura, T. Ogawa, N. Ogita, A new algorithm for three-dimensional Voronoi tessellation, Journal of Computational Physics 51 (2) (1983) 191–207. doi:10.1016/0021-9991(83)90087-6.

[67] Y. Cheng, A. J. Cao, H. Sheng, E. Ma, Local order influences initiation of plastic flow in metallic glass: Effects of alloy composition and sample cooling history, Acta Materialia 56 (18) (2008) 5263–5275. doi:10.1016/j.actamat.2008.07.011.

[68] A. Sharma, P. Singh, D. D. Johnson, P. K. Liaw, G. Balasubramanian, Atomistic clustering-ordering and high-strain deformation of an $Al_{0.1}$CrCoFeNi high-entropy alloy, Scientific Reports 6. doi:10.1038/srep31028.

[69] M. Jafary-Zadeh, R. Tavakoli, D. J. Srolovitz, Y.-W. Zhang, Thermally induced failure mechanism transition and its correlation with short-range order evolution in metallic glasses, Extreme Mechanics Letters 9 (2016) 215–225. doi:10.1016/j.eml.2016.07.009.

[70] C. A. Schuh, T. C. Hufnagel, U. Ramamurty, Mechanical behavior of amorphous alloys, Acta Materialia 55 (12) (2007) 4067–4109. doi:10.1016/j.actamat.2007.01.052.

[71] H. Sheng, E. Ma, M. J. Kramer, Relating dynamic properties to atomic structure in metallic glasses, Jom 64 (7) (2012) 856–881. doi:10.1007/s11837-012-0360-y.

[72] G. Duan, D. Xu, Q. Zhang, G. Zhang, T. Cagin, W. L. Johnson, W. A. Goddard III, Molecular dynamics study of the binary $Cu_{46}Zr_{54}$ metallic glass motivated by experiments: Glass formation and atomic-level structure, Physical Review B 71 (22) (2005) 224208. doi:10.1103/PhysRevB.71.224208.

[73] M. Heggen, F. Spaepen, M. Feuerbacher, Creation and annihilation of free

volume during homogeneous flow of a metallic glass, Journal of Applied Physics 97 (3) (2005) 033506. doi:10.1063/1.1827344.

[74] M. Li, M. Jiang, S. Yang, F. Jiang, L. He, J. Sun, Effect of strain rate on yielding strength of a zr-based bulk metallic glass, Materials Science and Engineering: A 680 (2017) 21–26. doi:10.1016/j.msea.2016.10.081.